Arteriosclerosis, Thrombosis, and Vascular Biology

JOURNAL OF THE AMERICAN HEART ASSOCIATION

Spontaneous Adult-Onset Pulmonary Arterial Hypertension Attributable to Increased Endothelial Oxidative Stress in a Murine Model of Hereditary Hemorrhagic Telangiectasia

Mourad Toporsian, Mirjana Jerkic, Yu-Qing Zhou, Mohammed G. Kabir, Lisa X. Yu, Brendan A.S. McIntyre, Adrienne Davis, Yu Jing Wang, Duncan J. Stewart, Jaques Belik, Mansoor Husain, Mark Henkelman and Michelle Letarte

Arterioscler Thromb Vasc Biol 2010;30;509-517; originally published online Dec 30, 2009;
DOI: 10.1161/ATVBAHA.109.200121
Arteriosclerosis, Thrombosis, and Vascular Biology is published by the American Heart Association. 7272 Greenville Avenue, Dallas, TX 72514
 Print ISSN: 1079-5642. Online ISSN: 1524-4636

Spontaneous Adult-Onset Pulmonary Arterial Hypertension Attributable to Increased Endothelial Oxidative Stress in a Murine Model of Hereditary Hemorrhagic Telangiectasia

Mourad Toporsian, Mirjana Jerkic, Yu-Qing Zhou, Mohammed G. Kabir, Lisa X. Yu, Brendan A.S. McIntyre, Adrienne Davis, Yu Jing Wang, Duncan J. Stewart, Jaques Belik, Mansoor Husain, Mark Henkelman, Michelle Letarte

Objective—Loss-of-function mutations in genes coding for transforming growth factor-β/bone morphogenetic protein receptors and changes in nitric oxide• ($NO^{\bullet}$) bioavailability are associated with hereditary hemorrhagic telangiectasia and some forms of pulmonary arterial hypertension. How these abnormalities lead to seemingly disparate pulmonary pathologies remains unknown. Endoglin (Eng), a transforming growth factor-β coreceptor, is mutated in hereditary hemorrhagic telangiectasia and involved in regulating endothelial $NO^{\bullet}$ synthase (eNOS)-derived $NO^{\bullet}$ production and oxidative stress. Because some patients with pulmonary arterial hypertension harbor *ENG* mutations leading to haplo insufficiency, we investigated the pulmonary vasculature of $Eng^{+/-}$ mice and the potential contribution of abnormal eNOS activation to pulmonary arterial hypertension.

Methods and Results—Hemodynamic, histological, and biochemical assessments and x-ray micro-CT imaging of adult $Eng^{+/-}$ mice indicated signs of pulmonary arterial hypertension including increased right ventricular systolic pressure, degeneration of the distal pulmonary vasculature, and muscularization of small arteries. These findings were absent in 3-week-old $Eng^{+/-}$ mice and were attributable to constitutively uncoupled eNOS activity in the pulmonary circulation, as evidenced by reduced eNOS/heat shock protein 90 association and increased eNOS-derived superoxide ($^{\bullet}O_2^-$) production in a BH_4-independent manner. These changes render eNOS unresponsive to regulation by transforming growth factor-β/bone morphogenetic protein and underlie the signs of pulmonary arterial hypertension that were prevented by Tempol.

Conclusion—Adult $Eng^{+/-}$ mice acquire signs of pulmonary arterial hypertension that are attributable to uncoupled eNOS activity and increased $^{\bullet}O_2^-$ production, which can be prevented by antioxidant treatment. Eng links transforming growth factor/bone morphogenetic protein receptors to the eNOS activation complex, and its reduction in the pulmonary vasculature leads to increased oxidative stress and pulmonary arterial hypertension. **(*Arterioscler Thromb Vasc Biol*. 2010;30:509-517.)**

Key Words: Alk-1 ■ endoglin ■ free radicals ■ nitric oxide ■ pulmonary arterial hypertension ■ transforming growth factor

Endoglin (Eng; CD105) is a an ancillary receptor for several transforming growth factor (TGF)-β superfamily ligands, including bone morphogenetic proteins (BMP).[1] It is predominantly expressed on vascular endothelial cells[2] and found in both TGF-β and BMP receptor complexes,[1,3] where it modulates TGF-β1/β3[4] and BMP9/10 effects,[5] respectively, via its physical association with the activin-like kinase receptor-1 (*ACVLR1*) gene product, ALK1. *Eng*-null mice die at mid-gestation with impaired angiogenesis and severe cardiac defects.[6,7] Whereas $Eng^{+/-}$ mice have a normal lifespan, they display abnormal systemic vascular autoregulatory functions related to endothelial nitric oxide synthase (eNOS) activity.[8]

Mutations in the endoglin (*ENG*) and activin-like kinase 1 receptor (*ACVLR1*) genes lead to haploinsufficiency and are the underlying cause of hereditary hemorrhagic telangiectasia type 1 (HHT1)[9] and type 2 (HHT2),[10] respectively. This disease is characterized by multiple focal telangiectases and arteriovenous malformations (AVMs) in the pulmonary, hepatic, and cerebral microcirculations.[11] These fragile structures are low-pressure conduits that can affect local tissue blood flow, and their

Received July 3, 2009; revision accepted December 8, 2009.

From the Molecular Structure and Function Program (M.T., M.J., A.D., Y.J.W., M.L.), Mouse Imaging Centre (Y.-Q.Z., L.X.Y., M.H.), Department of Pediatrics (B.A.S.M., J.B.), The Hospital for Sick Children, Toronto, Canada; Heart and Stroke Richard Lewar Center of Excellence (M.T., M.J., M.G.K., M.H., M.L.), Department of Immunology (M.T., M.L.), Department of Medical Biophysics (M.H., M.L.), University of Toronto, Toronto, Canada; Division of Pulmonary, Critical Care and Sleep Medicine (M.T.), Department of Medicine, Beth Israel Deaconess Medical Center, Harvard Medical School, Boston, Mass. Ottawa Health Research Institute (D.J.S.), University of Ottawa, Canada; Division of Cellular & Molecular Biology (M.G.K., M.H.), Toronto General Hospital, Toronto, Canada.

M.T. and M.J. have equally contributed data to this work.

Correspondence to Dr Mourad Toporsian, Beth Israel Deaconess Medical Center, Department of Medicine, Division of Pulmonary, Critical Care and Sleep Medicine, Center for Vascular Biology Research, 99 Brookline Avenue, RN-233, Boston, MA 02115. E-mail mtoporsi@bidmc.harvard.edu

Arterioscler Thromb Vasc Biol **is available at http://atvb.ahajournals.org** **DOI: 10.1161/ATVBAHA.109.200121**

potential rupture in vital organs may lead to internal hemorrhage, anemia, and death. Patients with HHT1 and HHT2 display phenotypically similar vascular lesions but diverge with respect to organ involvement with a higher prevalence of pulmonary arteriovenous malformations (PAVMs) in HHT1.[12]

Mutations in *ACVRL1* have also been reported in patients presenting with pulmonary arterial hypertension (PAH),[13–15] suggesting that HHT and PAH may share defects in related signaling pathways. PAH is characterized by a sustained elevation in mean pulmonary arterial pressure causing progressive right ventricular hypertrophy and leading to heart failure and death.[16] The increase in pulmonary arterial pressure is attributable to increased pulmonary vascular resistance (PVR) caused by progressive loss/pruning of the peripheral lung vasculature and muscularization of small arterioles. Similar to HHT,[8] patients and animal models with pulmonary hypertension show endothelial dysfunction from changes in $NO^{\bullet}$ bioavailability attributable to increased oxidative stress in the pulmonary vasculature.[16–18] eNOS activity is reduced in hypoxia-induced pulmonary hypertension as a result of impaired association of eNOS with its allosteric regulator, heat shock protein 90 (Hsp90).[19] Such changes in eNOS activation were shown to lead to increased eNOS-derived reactive oxygen species (ROS) generation instead of $NO^{\bullet}$ in endothelial cells,[20] and the resulting oxidant stress contributes to an animal model of persistent pulmonary hypertension of the newborn.[21,22] Whereas loss-of-function mutations in TGF-β/BMP receptors have been associated with familial forms of PAH, the contributions of abnormal eNOS biology and endothelial oxidative stress in these forms of PAH remain to be elucidated.

We report that adult $Eng^{+/-}$ mice spontaneously develop signs of PAH that are attributable to uncoupled eNOS activity and ROS production causing progressive loss in pulmonary vascularity and increased muscularization of arterioles. Eng links TGF-β/BMP receptors to the eNOS activation complex, where its reduction leads to constitutive endothelial eNOS-derived oxidative stress, rendering the enzyme unresponsive to regulation by TGF-β/BMP signaling. These changes underlie PAH in $Eng^{+/-}$ mice, which can be prevented by treatment with Tempol.

Materials and Methods

Animal Studies

All experimental protocols were performed in accordance with the Canadian Council on Animal Care and approved by the Animal Care Committee of the Hospital for Sick Children. N17-N19 $Eng^{+/-}$ and $Eng^{+/+}$ C57BL/6 mice were generated by Dr Letarte at the Hospital for Sick Children by successive backcrosses. Mice ranging from 3 to 18 weeks old were used; 8- to 12-week-old mice were exposed to hypoxia (12% O_2) for 3 weeks in a Plexiglas chamber or to room air (21% O_2). In separate experiments, 3-week-old $Eng^{+/-}$ and $Eng^{+/+}$ mice were exposed to 1 mmol/L Tempol (4-hydroxy-2,2,6,6-tetramethypiperidine-1-oxyl; Fluka) in the drinking water for 6 weeks. Mice were anesthetized with 1.5% isoflurane for hemodynamic measurements or euthanized for lung histology, x-ray micro-CT, and biochemical studies.

Cardiac Measurements

Peak right ventricular systolic pressure (RVSP) was measured in mice by Millar Mikro-tip pressure transducer catheterization of the right ventricle (RV) via the external jugular vein (AD Instruments). The RV was dissected from the left ventricle and septum, and the Fulton index (RV/left ventricle+septum weight ratio) was calculated.

Ultrasound Biomicroscopy

Using a Vevo 770 ultrasound biomicroscope (VisualSonics), observations of the mouse heart and great vessels were conducted as described.[23] Dynamic changes in chamber/lumen dimensions were recorded using M-mode. RV stroke volume was calculated by multiplying the velocity–time integral by the main pulmonary artery cross-sectional area at peak systole. The isovolumetric contraction, relaxation, and ejection times were measured to calculate the Tei index=(isovolumetric contraction + isovolumetric relaxation IVRT)/ejection time.

Lung X-Ray Micro-CT

Anesthetized mice were intubated by tracheotomy and breathing was monitored using a pressure-controlled ventilator. Mice were perfused at 20 mm Hg via the RV with warm heparinized phosphate-buffered saline, followed by Microfil (Flow Tech) at 40 mm Hg using a pressure Servo System PS/200 (Living Systems Instrumentation). For 3-week-old mice, lungs were perfused at 10 mm Hg and with 3-fold diluted Microfil at 25 mm Hg. Specimens were scanned at 29 μm using a Micro-CT scanner (GE Healthcare). Three-dimensional volume data were reconstructed using the Feldkamp algorithm for cone-beam CT geometry. Three-dimensional isosurface rendering of the pulmonary vasculature was accomplished using MicroView software (GE Healthcare).

Morphometric Analysis of Small Arteries in Lungs

Paraffin-embedded transverse lung sections of 8- to 12-week-old and 18-week-old mice were stained with Movat's pentachrome, and 5 independent fields were quantified for the number of small arteries per 100 alveoli. Average wall areas of arteries were determined from the difference between outer and inner wall areas for 20 vessels per section and averaged for each mouse.

Lung ROS Measurements

Lungs were homogenized in phosphate-buffered Krebs containing 1 mmol/L NaN_3, and ROS levels were assessed using 10 μmol/L 5-(and6-)-caboxy-2-,7-dichloro dihydrofluorescein diacetate (carboxy-H_2DCFDA; Molecular Probes) at 37°C. Fluorescence was quantified on a SpectraMax spectrofluorometer (Molecular Devices) using 488 nm excitation and 525 nm emission wavelengths and was normalized for protein content.

Lung $NO^{\bullet}$ Measurements

Excised lung tissue was incubated in Krebs-Henseleit buffer for 2 hours at 37°C in the presence and absence of L-NAME. $NO^{\bullet}$ production was quantified using an $NO^{\bullet}$ microsensor ISO-NOP700 attached to an Apollo 4000 Free Radical Analyzer. The microsensor was calibrated using S-Nitroso-N-acetylpenicillamine in the presence of copper sulfate.

eNOS/Hsp90 Association and Immunoblotting

Lung segments were stimulated with vehicle or 1 μmol/L ionomycin for 15 minutes. Mouse $Eng^{+/+}$ and $Eng^{-/-}$ endothelial cells derived from the yolk sac of E8.5 embryos[8,24] were stimulated with increasing concentrations of TGF-β1. Extracts were prepared in 10 mmol/L Tris-HCl (pH=7.4; 1% Triton X-100 with protease/phosphatase inhibitors) and precleared with protein A/G mixture. eNOS homodimer formation in lung extracts were performed by low-temperature SDS-PAGE. Proteins were immunoprecipitated or immunoblotted with antibodies to phospho-eNOS Thr495, eNOS, Hsp90, b-actin (BD Biosciences), and Eng (MJ7/18, Southern Biotech) or Alk1 (Santa Cruz Biotech). Bands were visualized by chemiluminescence and quantified.

NOS-Derived O_2^- Measurements

eNOS-derived ROS levels were assessed by dihydroethidium (DHE; Molecular Probes) staining in isolated main pulmonary

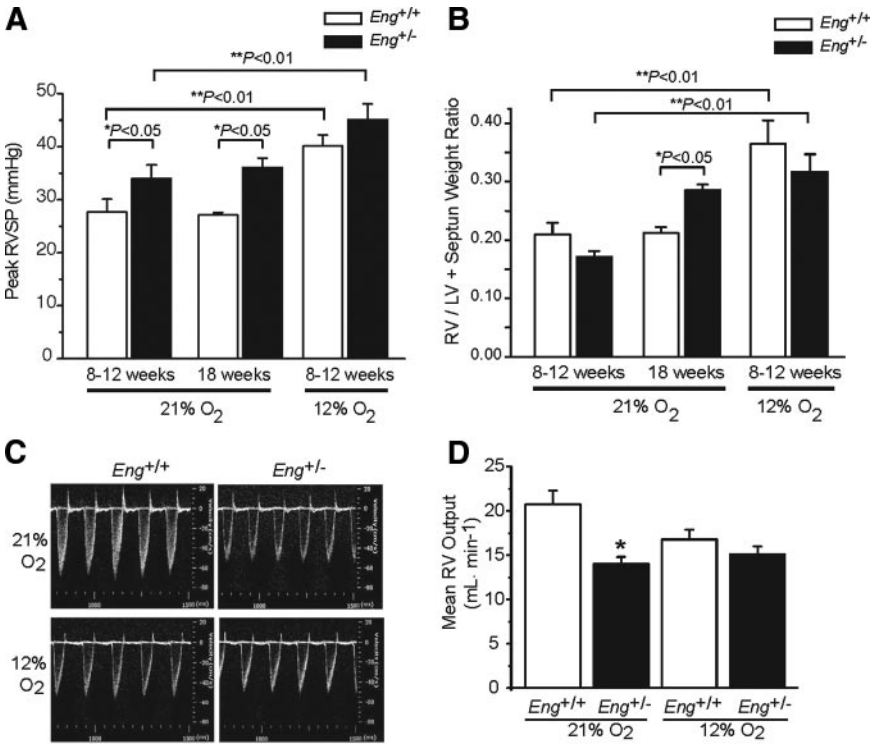

Figure 1. Increased RVSP in normoxic $Eng^{+/-}$ mice. A, Elevated RVSP in 8- to 12-week-old and 18-week-old $Eng^{+/-}$ mice compared to $Eng^{+/+}$, and RVSP increased to the same level in both groups of mice exposed to 12% O_2 (n=11/group; *P<0.05 vs normoxic $Eng^{+/+}$ mice; #P<0.05 vs $Eng^{+/-}$ normoxic mice). B, RV/left ventricle plus septum was unchanged in normoxic 8- to 12-week-old $Eng^{+/-}$ but elevated in 18-week-old $Eng^{+/-}$ vs littermate $Eng^{+/+}$ (n=11/group; *P<0.05). This parameter was significantly increased in both groups of mice after hypoxia. C, Representative Doppler images showing main pulmonary artery velocity time profiles in $Eng^{+/+}$ and $Eng^{+/-}$ mice exposed to 21% or 12% O_2. D, $Eng^{+/-}$ mice displayed reduced RV output compared to $Eng^{+/+}$ littermates (*P<0.05). RV output was similar in both groups of mice after hypoxia.

arteries. After preincubation with and without L-NAME (10^{-3} mol/L), vessels were incubated with acetylcholine (ACh, 10^{-5} mol/L) and 2 μmol/L DHE at 37°C. Vessels were washed, mounted *en face* on glass slides exposing the endothelial layer, and analyzed by fluorescence microcopy.

$Eng^{+/+}$ and $Eng^{-/-}$ embryonic endothelial cells were grown in Optilux 96-well black clear-bottom plates and serum-starved for 3 hours. Cells were incubated with 5 μmol/L DHE in the presence and absence of L-NAME and stimulated with 1 μmol/L ionomycin. Live cells were observed through the CY3 fluorescence channel and photographed using a TE2000 inverted microscope (Nikon) equipped with an environmental chamber set to 37°C and 5% CO_2. The number of positive nuclei/field was quantified based on size and intensity using 3-dimensional imaging software (Volocity).

Lung BH_4 and BH_2 Measurements

Lungs were homogenized in 50 mmol/L phosphate buffer (pH 2.6) containing 0.1 mmol/L DTPA and 1 mmol/L DTE. Samples were loaded onto a high-performance liquid chromatography system (CoulArray system, Model 582 and 542; ESA Biosciences) with a Synergi Polar-RP column (4 μ; 250×4.6 mm; Phenomenex) and eluted with argon-saturated 50 mmol/L phosphate buffer (pH 2.6). Calibration curves were made by summing up the peak areas collected at 0 and 150 mV for BH_4 and 280 and 365 mV for BH_2. Intracellular concentrations were calculated using authentic BH_4 and BH_2 (10 to 100 nmol/L) as standards and normalized to protein content.

eNOS Activity

Cultured $Eng^{+/+}$ and $Eng^{-/-}$ endothelial cells were preincubated with and without L-NAME and NOS activity was assayed by monitoring the conversion of ^{3}H-L-arginine to ^{3}H-L-citrulline in response to TGF-β1 (250 pmol/L), as previously described.[8]

Statistical Analysis

Comparisons were performed by 1- or 2-way ANOVA, and significant overall differences were evaluated posthoc using the Bonferroni procedure. Results are expressed as the mean±SEM, with P<0.05 representing significance.

Results

$Eng^{+/-}$ Mice Have Elevated RVSP and RV Hypertrophy

The 8- to 12-week-old $Eng^{+/-}$ mice had elevated RVSP reaching 33.9±2.6 mm Hg vs 27.6±2.6 mm Hg in control $Eng^{+/+}$ mice (Figure 1A; P<0.05). In 18-week-old mice, this parameter was unchanged in the $Eng^{+/+}$ group (27.1±0.5 mm Hg) but significantly increased to 36.1±1.8 in the $Eng^{+/-}$ group. Exposure to the pulmonary hypertension-inducing stimulus,12% O_2 for 3 weeks, resulted in similarly elevated RVSP (P<0.01 vs normoxic mice) in $Eng^{+/+}$ (40.1±2.1 mm Hg) and $Eng^{+/-}$ mice (45.1±2.9 mm Hg). $Eng^{+/-}$ mice had normal heart rates (412±42 vs 442±31 bpm), mean systemic arterial pressures (87.4±2.8 vs 90.4±3.9 mm Hg), body weights, and activity levels. RV hypertrophy was not observed in 8- to 12-week-old mice but was seen in 18-week-old normoxic $Eng^{+/-}$ mice (Figure 1B), suggesting that a longer exposure to elevated RV load was necessary for this manifestation. Similar levels of RV hypertrophy were noted in $Eng^{+/+}$ and $Eng^{+/-}$ mice after hypoxia (P>0.05), consistent with the increased RVSP. Left ventricle plus septum weights did not vary between groups and the RV-to-body weight ratios confirmed the RV hypertrophy determined by the Fulton index. Whereas absolute Eng levels were increased after hypoxia (P<0.01), relative levels between $Eng^{+/-}$ and $Eng^{+/+}$ mice remained unchanged (Supplemental Figure IA, available online at http://atvb.ahajournals.org).

Doppler flow velocity spectra in the main pulmonary artery were recorded using ultrasound biomicroscopy (Figure 1C), and reduced RV output (Figure 1D) was determined for $Eng^{+/-}$ mice (P<0.05 vs $Eng^{+/+}$). Hypoxia reduced RV

output in $Eng^{+/+}$ mice but did not further affect this parameter in $Eng^{+/-}$ mice. The calculated RV Tei index and RV fractional shortening were unchanged in normoxic $Eng^{+/-}$ mice, suggesting normal RV function (Supplemental Figure IIA, IIB, available online at http://atvb.ahajournals.org). Moreover, left ventricle function was normal in $Eng^{+/-}$ mice, as evidenced by unchanged percent fractional shortening (27.9±1.3 vs 25.9±1.9), isovolumetric contraction time-to-ejection time ratio (0.22±0.01 vs 0.22±0.02), and isovolumetric relaxation time-to-filling time ratio (0.28±0.01 vs 0.27±0.01).

Adult $Eng^{+/-}$ Mice Show Reduced Pulmonary Vascular Density

Pulmonary circulation of 3-week-old $Eng^{+/-}$ mice was analyzed by x-ray micro-CT and found to be normal (Figure 2A). In contrast, 8- to 12-week-old $Eng^{+/-}$ mice displayed enlarged main pulmonary arteries and pruning of peripheral vessels (Figure 2B), suggesting that these features were acquired in adult $Eng^{+/-}$ mice. The absence of Microfil in pulmonary veins of $Eng^{+/-}$ mice suggested increased resistance to flow in distal pulmonary arterioles and lack of large arteriovenous shunts. The number of pulmonary arteries (<60 μm) per 100 alveoli was reduced in normoxic 8- to 12-week-old and 18-week-old $Eng^{+/-}$ mice compared to age-matched controls (Figure 2C; $P<0.05$). Exposure to hypoxia reduced arterial density in both $Eng^{+/+}$ and $Eng^{+/-}$ mice to the same extent, whereas alveolar density remained unchanged (Figure 2C). Lung sections of 7-day-old $Eng^{+/+}$ and $Eng^{+/-}$ mice showed similar vessel and alveoli densities, indicating no detectable congenital defects in lung size, angiogenesis, or alveolarization (data not shown).

Our inability to effectively perfuse the venous system via the pulmonary artery in adult $Eng^{+/-}$ mice suggested increased resistance to flow in distal pulmonary arteries. Movat's pentachrome staining revealed significant muscularization of small arterioles in adult $Eng^{+/-}$ vs $Eng^{+/+}$ mice. This phenotype was observed in both groups of mice after hypoxia. Muscularization of arteries was confined to the <30-μm group in the 8- to 12-week-old normoxic $Eng^{+/-}$ group (Figure 2D; $P<0.05$ vs control). However, in 18-week-old $Eng^{+/-}$ mice, wall thickening was observed in <30-μm and >40-μm arteries, indicating more widespread remodeling with age. After hypoxia, no difference in vessel wall area was observed between $Eng^{+/-}$ and control mice, and all vessels displayed increased wall area compared to those from normoxic mice. For each vessel caliber, internal diameters were unchanged (data not shown), indicating outward remodeling of $Eng^{+/-}$ blood vessels and suggesting that increased PVR was contributed by reduced vascularity and changes in local vasomotor tone. Some vessels harbored fibrin clots/thrombi, a feature observed in both PAH and HHT (Supplemental Figure IIIA, available online at http://atvb.ahajournals.org). Some older $Eng^{+/-}$ mice also displayed AVM-like structures with notable arterialization of veins (Supplemental Figure IIIB).

Increased ROS Production and Uncoupled eNOS Activity in $Eng^{+/-}$ Pulmonary Vasculature

Total ROS production in lungs of mice was assessed and shown to be significantly elevated in $Eng^{+/-}$ lungs compared

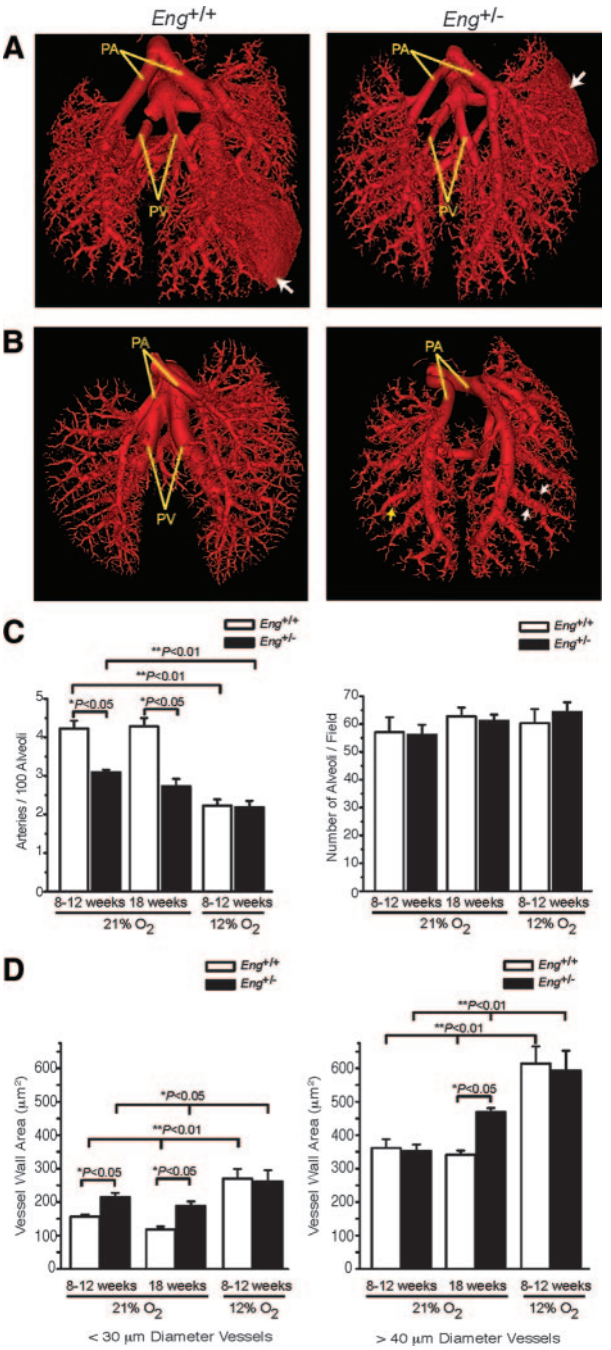

Figure 2. Reduced pulmonary vascular density in adult $Eng^{+/-}$ mice. A, Similar representative x-ray micro-CT images of 3-week-old $Eng^{+/+}$ and $Eng^{+/-}$ mice showing the right/left main pulmonary arteries (PA) and veins (PV) (yellow arrows). Areas of overperfusion attributable to rupture of the vasculature are indicated by white arrows. B, Representative images of 8-week-old mice showing enlarged $Eng^{+/-}$ left and right main PA and smaller-caliber PA (yellow arrows). PV were perfused in $Eng^{+/+}$ but not in $Eng^{+/-}$ mice. Pruning of small peripheral arteries was observed in the $Eng^{+/-}$ mice (white arrows). C, The 8- to 12-week-old and 18-week-old $Eng^{+/-}$ mice have decreased number of arteries per 100 alveoli compared to age-matched $Eng^{+/+}$controls (*$P<0.05$; n=6/group). Hypoxia (12% O_2) decreased lung arterial density in both groups (n=6/group) while having no effect on the number of alveoli per field. D, Increased vessel wall area in <30-μm diameter vessels in normoxic 8-to 12-week-old $Eng^{+/-}$ mice. Larger-caliber vessels (>40 μm) were affected in 18-week-old $Eng^{+/-}$ mice (*$P<0.05$ vs normoxic $Eng^{+/+}$; n=6/group). Wall areas of all vessels were increased in both groups of mice (n=6/group) after hypoxia.

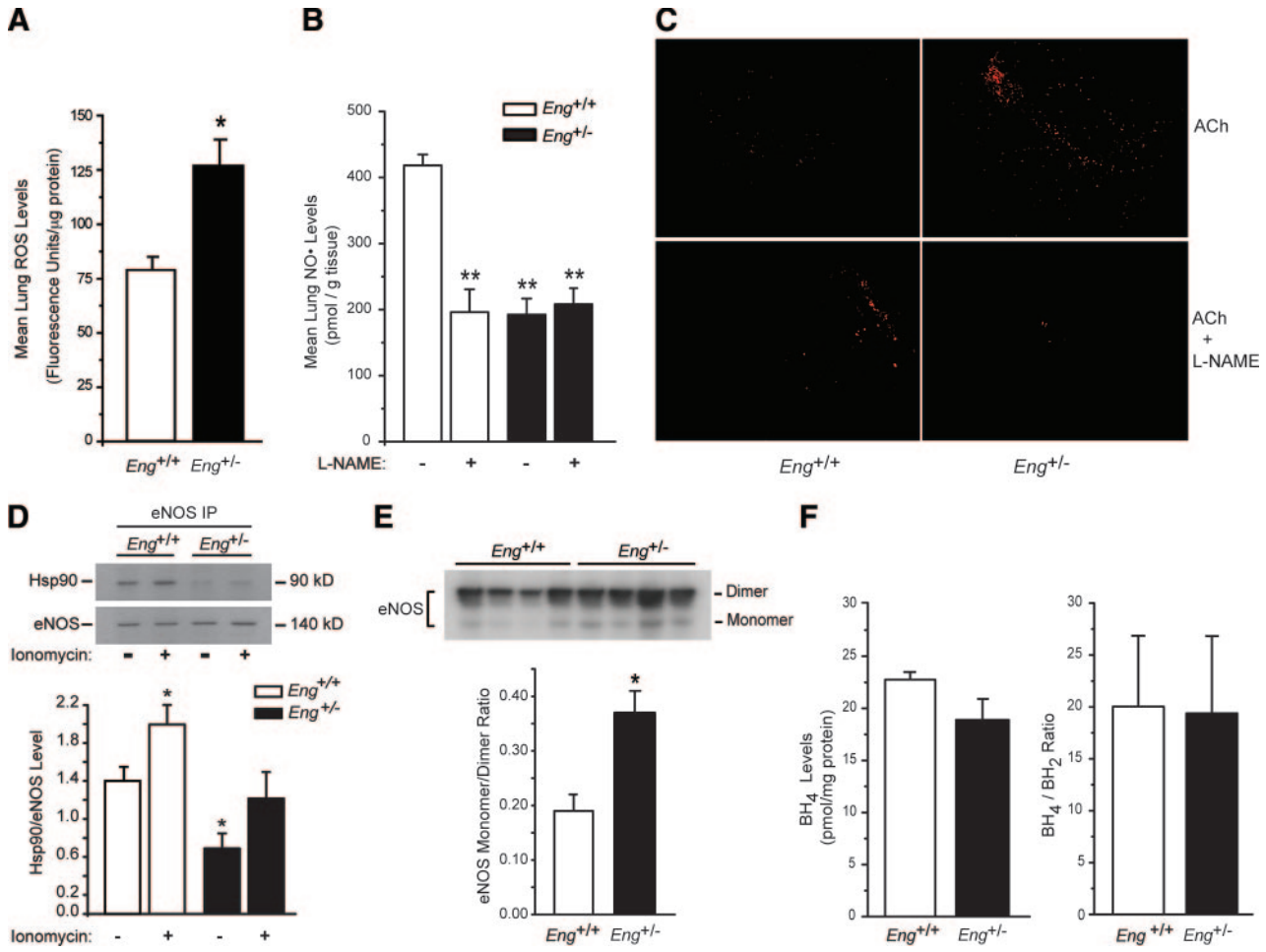

Figure 3. ROS production and uncoupled eNOS activity in *Eng*$^{+/-}$ lung vasculature. A, *Eng*$^{+/-}$ lungs produced significantly greater amount of ROS (**P*<0.05 vs *Eng*$^{+/+}$). B, Lack of L-NAME–inhibitable NO• production in *Eng*$^{+/-}$ lungs (***P*<0.01 vs untreated *Eng*$^{+/+}$; n=5/group). C, Representative images showing increased acetylcholine-induced DHE staining in *Eng*$^{+/-}$ vs *Eng*$^{+/+}$ pulmonary arteries. L-NAME abrogated this response in *Eng*$^{+/-}$ arteries but enhanced DHE staining in *Eng*$^{+/+}$ arteries, probably by inhibiting the normal $^{\bullet}O_2^-$ scavenging by NO•. D, Representative immunoprecipitation/Western blot and graph showing increased Hsp90 levels in eNOS immunoprecipitates of *Eng*$^{+/+}$ lungs, but not *Eng*$^{+/-}$ lungs, stimulated with ionomycin (**P*<0.05 vs untreated). Basal eNOS/Hsp90 association was also reduced in *Eng*$^{+/-}$ lung samples (#*P*<0.05 vs untreated *Eng*$^{+/+}$; n=4/group). E, Representative Western blot and graph showing increased ratio of eNOS monomer to dimer levels in lung extracts of *Eng*$^{+/-}$ (**P*<0.05 vs *Eng*$^{+/+}$ mice; n=5/group). F, Unchanged BH_4 levels and BH_4-to-BH_2 ratio in *Eng*$^{+/-}$ lungs.

to *Eng*$^{+/+}$ littermates (Figure 3A; *P*<0.05). Unlike *Eng*$^{+/+}$ mice, lungs of *Eng*$^{+/-}$ mice did not display any L-NAME–inhibitable NO• production, suggesting abnormal eNOS activation and potential uncoupling (Figure 3B). Increased eNOS-derived ROS production was examined in pulmonary arteries (PA) by *en face* DHE staining of the endothelium in response to ACh. Compared to *Eng*$^{+/+}$ PA, those of *Eng*$^{+/-}$ mice displayed increased endothelial DHE staining, confirming ROS generation, which was abolished by L-NAME (Figure 3C). Very little DHE staining was observed in ACh-stimulated *Eng*$^{+/+}$ arteries, and L-NAME had an enhancing effect, likely attributable to the loss of ROS scavenging activity of NO•. These results were substantiated by reduced eNOS/Hsp90 association in *Eng*$^{+/-}$ vs *Eng*$^{+/+}$ lungs (Figure 3D) under basal conditions and after stimulation with ionomycin. Total eNOS and Hsp90 levels remained unchanged in *Eng*$^{+/-}$ vs *Eng*$^{+/+}$ lungs (Supplemental Figure IB, IC). However, the ratio of eNOS monomer to dimer levels was significantly higher in lung extracts of *Eng*$^{+/-}$ vs *Eng*$^{+/+}$ mice (Figure 3E), whereas lung BH_4 levels or the BH_4-to-BH_2 ratio remained unchanged (Figure 3F). Taken together, these data suggest that eNOS does not produce NO• in the lungs of *Eng*$^{+/-}$ mice and instead predominantly contributes to ROS production via uncoupling of its dimeric form in a BH_4-independent manner.

Tempol Prevents Onset of PAH in Adult *Eng*$^{+/-}$ Mice

Treatment of 3-week-old *Eng*$^{+/+}$ and *Eng*$^{+/-}$ mice with Tempol prevented the expected increase in RVSP (Figure 4A) in adult *Eng*$^{+/-}$ mice, as well as the outward arterial remodeling (Figure 4B), the rarefaction of distal arterioles (Figure 4C), and the increase in vessel wall area (Figure 4D).

Eng Links TGF-β/BMP Signaling to eNOS

Eng immunoprecipitates with eNOS,[8] suggesting that eNOS activation may be regulated by TGF-β/BMP receptor signaling. We now report that ALK1 can also be immunoprecipi-

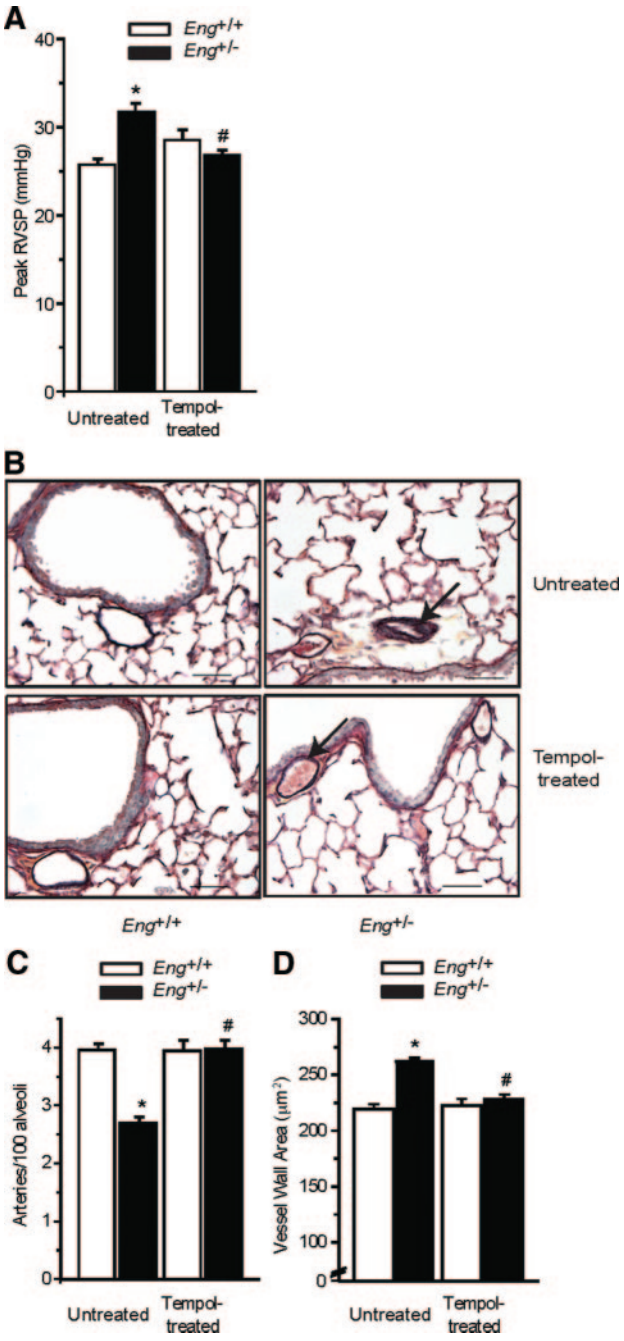

Figure 4. Tempol prevents onset of PAH in $Eng^{+/-}$ mice. A, Elevated RVSP in 9-week-old $Eng^{+/-}$ mice (*$P<0.05$ vs $Eng^{+/+}$) was prevented by Tempol (#$P<0.05$ vs untreated $Eng^{+/-}$). B, Representative Movat's pentachrome—stained lung sections from untreated and Tempol-treated $Eng^{+/+}$ and $Eng^{+/-}$ mice. Tempol caused normalization (C) of pulmonary artery (<60 μm) density and attenuation (D) of pulmonary vessel wall area (#$P<0.05$ vs untreated $Eng^{+/-}$). n=7–9 mice per group.

tated in a complex with eNOS (Figure 5A). TGF-β1, which acts through Eng and ALK1 in endothelial cells, stimulated eNOS/Hsp90 association in $Eng^{+/+}$ but not in $Eng^{-/-}$ cells (Figure 5B); TGF-β1 increased eNOS activity in $Eng^{+/+}$ cells but had no effect on $Eng^{-/-}$ cells, as measured by the rate of ^{3}H-L-citrulline production (Figure 5C). TGF-β1 also rapidly induced dephosphorylation of eNOS Thr495, a response impaired in $Eng^{-/-}$ cells (Figure 5D). These findings suggest that Eng is critical for eNOS activation by TGF-β1 and possibly other ligands of the TGF-β superfamily.

Constitutive eNOS-Derived ROS Production in Eng-Deficient Endothelial Cells

Our finding that Eng was required for both TGF-β–induced and ionomycin-induced stimulation of eNOS suggested constitutive eNOS uncoupling in Eng-deficient cells, independent of TGF-β/BMP receptors. Compared to mouse $Eng^{+/+}$ endothelial cells, a significantly greater number of $Eng^{-/-}$ cells showed nuclear DHE staining that was inhibitable with L-NAME under basal conditions, suggesting constitutive eNOS-derived ROS production (Figure 5E). Ionomycin significantly increased ROS production in $Eng^{+/+}$ but not $Eng^{-/-}$ cells. Pretreatment with L-NAME attenuated the ionomycin effect in both groups of cells (Figure 5E).

Discussion

Loss-of-function mutations in TGF-β/BMP receptors and endothelial oxidative stress have been associated with PAH. However, a functional inter-relationship between these alterations in PAH pathogenesis remains unknown. We have found that adult $Eng^{+/-}$ mice spontaneously develop signs of PAH because of endothelial dysfunction leading to progressive pruning of the pulmonary vasculature and muscularization of small arteries. Both in vivo and in vitro biochemical data suggest that PAH in $Eng^{+/-}$ mice is associated with an intrinsic defect in eNOS activation leading to constitutively increased eNOS-derived ROS production while rendering this enzyme refractory to regulation by members of the TGF-β/BMP superfamily. The onset of PAH in adult $Eng^{+/-}$ mice is prevented by treatment with the $^{\bullet}O_2^-$ dismutase mimetic, Tempol, underscoring the importance of eNOS uncoupling in this model of PAH.

Balancing eNOS-derived $NO^{\bullet}$ vs $^{\bullet}O_2^-$ production is an important determinant in numerous cardiovascular diseases, including PAH.[25–28] Interestingly, we observed increased eNOS-derived $^{\bullet}O_2^-$ production and were unable to detect any L-NAME–inhibitable $NO^{\bullet}$ generation in lungs of $Eng^{+/-}$ mice. Increased monomerization of eNOS was observed in $Eng^{+/-}$ lungs, which may partly account for the reduced $NO^{\bullet}$ production. Whereas it has been proposed that monomeric eNOS can produce $^{\bullet}O_2^-$, it has been recently shown that this is unlikely and that this form of the enzyme is inactive.[29] Interestingly, our finding that BH_4 levels remained unchanged in lung extracts of $Eng^{+/-}$ mice suggests that the observed increase in NOS-dependent $^{\bullet}O_2^-$ production occurs via the uncoupling of dimeric eNOS activity in a BH_4-independent manner. Taken together, these findings ascribe to Eng a critical role in modulating the eNOS activation complex.

Caveolin-1 null mice display signs of PAH attributable to persistent activation of eNOS leading to PKG nitration, a mechanism that necessitates both oxidative stress and heightened $NO^{\bullet}$ production.[30] Eng is enriched in caveolar lipid rafts, coimmunoprecipitates with caveolin-1 in endothelial cells, and regulates eNOS activation and $NO^{\bullet}$ bioavailability.[8] However, it is unlikely that PKG nitration plays a role in the PAH phenotype seen in $Eng^{+/-}$ mice, because we could not detect any L-NAME–inhibitable NO production. Perhaps

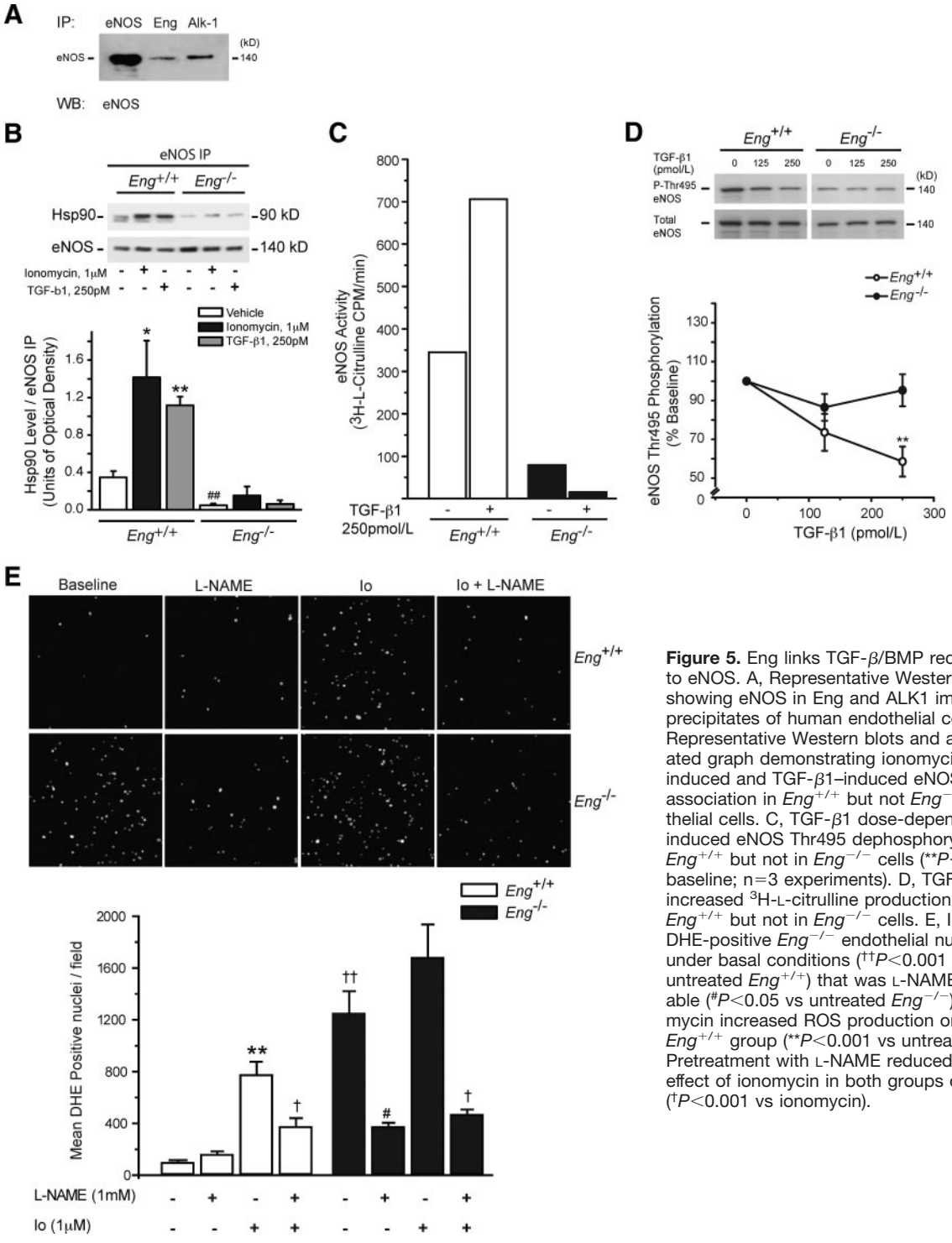

Figure 5. Eng links TGF-β/BMP receptors to eNOS. A, Representative Western blot showing eNOS in Eng and ALK1 immunoprecipitates of human endothelial cells. B, Representative Western blots and associated graph demonstrating ionomycin-induced and TGF-β1–induced eNOS/Hsp90 association in $Eng^{+/+}$ but not $Eng^{-/-}$ endothelial cells. C, TGF-β1 dose-dependently induced eNOS Thr495 dephosphorylation in $Eng^{+/+}$ but not in $Eng^{-/-}$ cells (**$P<0.01$ vs baseline; n=3 experiments). D, TGF-β1 increased ^{3}H-L-citrulline production in $Eng^{+/+}$ but not in $Eng^{-/-}$ cells. E, Increased DHE-positive $Eng^{-/-}$ endothelial nuclei under basal conditions (††$P<0.001$ vs untreated $Eng^{+/+}$) that was L-NAME–inhibitable (#$P<0.05$ vs untreated $Eng^{-/-}$). Ionomycin increased ROS production only in the $Eng^{+/+}$ group (**$P<0.001$ vs untreated). Pretreatment with L-NAME reduced the effect of ionomycin in both groups of cells (†$P<0.001$ vs ionomycin).

the difference between the 2 models is related to the balance of eNOS-derived NO• vs $^{\bullet}O_2^-$ and that the significant production of eNOS-derived $^{\bullet}O_2^-$ in $Eng^{+/-}$ mice is sufficient to induce PAH.

In adult $Eng^{+/-}$ mice, eNOS-derived ROS production and reduced NO• bioavailability likely reduced endothelial cell survival, leading to pruning of the distal pulmonary microvasculature and contributing to the muscularization of small arteries, effects that were prevented by the antioxidant, Tempol. We contend that the salutary effects of Tempol reported in the current study are likely attributable to its role in preserving NO• bioavailability by the dismutation of $^{\bullet}O_2^-$ to H_2O_2. NO• normally prevents excessive smooth muscle proliferation/remodeling and coordinates arterial repair.[31] Moreover, H_2O_2 likely served as an endothelium-derived hyperpolarizing factor of vascular smooth muscle, thus attenuating the increase in pulmonary vascular resistance and pressure. We believe excess $^{\bullet}O_2^-$, and not H_2O_2, leads to PAH in $Eng^{+/-}$ lungs and that endogenous $^{\bullet}O_2^-$ dismutase activities are relatively insufficient to prevent disease. Inter-

estingly, PAH is acquired in adult $Eng^{+/-}$ mice, suggesting an increased predisposition of these mice to age-related uncoupling of eNOS, a developmentally regulated phenomenon recently reported in piglets.[32]

Our finding that eNOS co-immunoprecipitates with both Eng and ALK1 further supports a central role for Eng in linking TGF-β/BMP receptors to eNOS. TGF-β1 caused increased eNOS/Hsp90 association, eNOS Thr495 dephosphorylation, and ^{3}H-L-arginine to ^{3}H-L-citrulline conversion in $Eng^{+/+}$, but not in $Eng^{-/-}$ endothelial cells. However, failure of the receptor-independent eNOS agonist, ionomycin, and of TGF-β1 to induce eNOS/Hsp90 association in Eng-deficient cells suggests an intrinsic defect in eNOS activation. This is supported by our findings of significantly elevated eNOS-derived ROS production in unstimulated $Eng^{-/-}$ cells, indicating constitutive uncoupling and thus rendering eNOS refractory to regulation by TGF-β1/BMP and other ligands in this superfamily.

Our study supports clinical observations in which HHT patients manifest PAVMs and varying degrees of pulmonary hypertension,[15,33,34] suggesting a common defective pathway involving Eng/ALK1 that predisposes to lesions associated with these diseases. We have found abnormal vascular structures suggestive of PAVMs in $Eng^{+/-}$ mice that also display PAH (Supplemental Figure III). We have previously reported that $Eng^{+/-}$ systemic arteries have a reduced ability to contract in response to elevations in transmural pressure, thus failing to effectively reduce vessel wall tension. Elevated parietal wall tension attributable to increased pulmonary perfusion pressure would increase the probability of PAVMs and their subsequent risk of rupture. Perhaps the observed enlargement of large feeding pulmonary arteries in $Eng^{+/-}$ may be a prelude to abnormal vascular structures reminiscent of HHT. We propose that small, low-resistance AVM-like structures may arise from elevated pulmonary vascular pressure and account for the relatively mild increase in RVSP and PAH progression in adult $Eng^{+/-}$ mice. Manifestations of PAH or HHT may be influenced by genetic and environmental modifying factors that specifically affect the integrity of the $Eng^{+/-}$ pulmonary vasculature and its ability for normal remodeling/repair undergoing elevated intravascular pressure. Interestingly, shRNA-mediated silencing of BMP receptor-2 in mice resulted in signs of HHT instead of the expected PAH.[35] More recently, conditional ablation of BMP receptor-2 in the pulmonary endothelium was sufficient to elicit signs of PAH only in a subset of mice.[36] It remains to be determined if the appearance of small PAVM-like structures may have counteracted the increase in RVSP and progression of PAH in the seemingly asymptomatic group of BMP receptor-2–deficient mice.

PAVMs are more prevalent in HHT1 than in HHT2 patients (48% vs 5%).[12] These low-resistance structures could alleviate overall PVR, providing a partial explanation for the higher prevalence of PAH in patients with *ACVRL1* vs *ENG* mutations.[15] Whereas a current study suggests that embolization of PAVMs does not lead to a sustained elevation in pulmonary arterial pressure in HHT patients,[34] this does not necessarily preclude an increased PVR because embolization can also be associated with reduced cardiac output. Patients with *ENG* mutations presenting with PAH typically have lower PVR than those with *ACVRL1* mutations.[4] Moreover, in some of these cases, the increased pulmonary arterial pressure is eventually normalized with the appearance of PAVMs.[13,37] Our findings suggest that *ENG* mutations leading to haploinsufficiency are a predisposing factor to PAH, and that PAVMs in HHT1 may result from abnormal vascular remodeling under high local pressure conditions that may, in turn, serve to alleviate PVR.

Our study ascribes to Eng a critical role in the maintenance of the mature lung vasculature. In adult $Eng^{+/-}$ mice, alterations in eNOS activation leading to uncoupling renders the enzyme refractory to regulation by TGF-β/BMP signaling and constitutes a critical event leading to excessive oxidative stress and PAH pathogenesis. The absence of disease in younger mice may be related to the prolonged time course required for PAH manifestations, or mechanisms surrounding eNOS uncoupling are developmentally regulated. Our study suggests a close association between PAH and HHT1, and our experimental system may provide a means to define the specific determinants in the pathogenesis of both diseases. Future genetic screening of families with PAH may unravel more individuals with *ENG* mutations.

Acknowledgments

The authors thank Jennifer Whitsett (Medical College of Wisconsin) for the BH_4/BH_2 measurements by high-performance liquid chromatography, and Aditi M. Jhaveri from the Beth Israel Deaconess Medical Center for technical support.

Sources of Funding

This work was supported by grants from the CIHR (MOP-6247), Heart & Stroke Foundation of Ontario (T5598), and the HHT International Foundation (contract #5) to M. Letarte; the Klarman Family Foundation and BIDMC/Department of Medicine Commitment Fund to M. Toporsian; CFI grant to M. Henkelman (2555); and CIHR grant to M. Husain (MOP-64352).

Disclosures

None.

References

1. Barbara NP, Wrana JL, Letarte M. Endoglin is an accessory protein that interacts with the signaling receptor complex of multiple members of the transforming growth factor-beta superfamily. *J Biol Chem*. 1999;274:584–594.
2. Gougos A, Letarte M. Primary structure of endoglin, an RGD-containing glycoprotein of human endothelial cells. *J Biol Chem*. 1990;265:8361–8364.
3. Blanco FJ, Santibanez JF, Guerrero-Esteo M, Langa C, Vary CP, Bernabeu C. Interaction and functional interplay between endoglin and ALK-1, two components of the endothelial transforming growth factor-beta receptor complex. *J Cell Physiol*. 2005;204:574–584.
4. Lastres P, Letamendia A, Zhang H, Rius C, Almendro N, Raab U, Lopez LA, Langa C, Fabra A, Letarte M, Bernabeu C. Endoglin modulates cellular responses to TGF-beta 1. *J Cell Biol*. 1996;133:1109–1121.
5. David L, Mallet C, Mazerbourg S, Feige JJ, Bailly S. Identification of BMP9 and BMP10 as functional activators of the orphan activin receptor-like kinase 1 (ALK1) in endothelial cells. *Blood*. 2007;109:1953–1961.
6. Bourdeau A, Dumont DJ, Letarte M. A murine model of hereditary hemorrhagic telangiectasia. *J Clin Invest*. 1999;104:1343–1351.
7. Li DY, Sorensen LK, Brooke BS, Urness LD, Davis EC, Taylor DG, Boak BB, Wendel DP. Defective angiogenesis in mice lacking endoglin. *Science*. 1999;284:1534–1537.
8. Toporsian M, Gros R, Kabir MG, Vera S, Govindaraju K, Eidelman DH, Husain M, Letarte M. A role for endoglin in coupling eNOS activity and

regulating vascular tone revealed in hereditary hemorrhagic telangiectasia. *Circ Res*. 2005;96:684–692.
9. McAllister KA, Grogg KM, Johnson DW, Gallione CJ, Baldwin MA, Jackson CE, Helmbold EA, Markel DS, McKinnon WC, Murrell J, et al. Endoglin, a TGF-beta binding protein of endothelial cells, is the gene for hereditary haemorrhagic telangiectasia type 1. *Nat Genet*. 1994;8: 345–351.
10. Berg JN, Gallione CJ, Stenzel TT, Johnson DW, Allen WP, Schwartz CE, Jackson CE, Porteous ME, Marchuk DA. The activin receptor-like kinase 1 gene: genomic structure and mutations in hereditary hemorrhagic telangiectasia type 2. *Am J Hum Genet*. 1997;61:60–67.
11. Guttmacher AE, Marchuk DA, White RI Jr. Hereditary hemorrhagic telangiectasia. *N Engl J Med*. 1995;333:918–924.
12. Letteboer TG, Mager JJ, Snijder RJ, Koeleman BP, Lindhout D, Ploos van Amstel JK, Westermann CJ. Genotype-phenotype relationship in hereditary haemorrhagic telangiectasia. *J Med Genet*. 2006;43:371–377.
13. Harrison RE, Berger R, Haworth SG, Tulloh R, Mache CJ, Morrell NW, Aldred MA, Trembath RC. Transforming growth factor-beta receptor mutations and pulmonary arterial hypertension in childhood. *Circulation*. 2005;111:435–441.
14. Harrison RE, Flanagan JA, Sankelo M, Abdalla SA, Rowell J, Machado RD, Elliott CG, Robbins IM, Olschewski H, McLaughlin V, Gruenig E, Kermeen F, Halme M, Raisanen-Sokolowski A, Laitinen T, Morrell NW, Trembath RC. Molecular and functional analysis identifies ALK-1 as the predominant cause of pulmonary hypertension related to hereditary haemorrhagic telangiectasia. *J Med Genet*. 2003;40:865–871.
15. Trembath RC, Thomson JR, Machado RD, Morgan NV, Atkinson C, Winship I, Simonneau G, Galie N, Loyd JE, Humbert M, Nichols WC, Morrell NW, Berg J, Manes A, McGaughran J, Pauciulo M, Wheeler L. Clinical and molecular genetic features of pulmonary hypertension in patients with hereditary hemorrhagic telangiectasia. *N Engl J Med*. 2001; 345:325–334.
16. Farber HW, Loscalzo J. Pulmonary arterial hypertension. *N Engl J Med*. 2004;351:1655–1665.
17. Grobe AC, Wells SM, Benavidez E, Oishi P, Azakie A, Fineman JR, Black SM. Increased oxidative stress in lambs with increased pulmonary blood flow and pulmonary hypertension: role of NADPH oxidase and endothelial NO synthase. *Am J Physiol Lung Cell Mol Physiol*. 2006; 290:L1069–L1077.
18. Wunderlich C, Schmeisser A, Heerwagen C, Ebner B, Schober K, Braun-Dullaeus RC, Schwencke C, Kasper M, Morawietz H, Strasser RH. Chronic NOS inhibition prevents adverse lung remodeling and pulmonary arterial hypertension in caveolin-1 knockout mice. *Pulm Pharmacol Ther*. 2008;21:507–515.
19. Murata T, Yamawaki H, Hori M, Sato K, Ozaki H, Karaki H. Hypoxia impairs endothelium-dependent relaxation in organ cultured pulmonary artery. *Eur J Pharmacol*. 2001;421:45–53.
20. Ou J, Fontana JT, Ou Z, Jones DW, Ackerman AW, Oldham KT, Yu J, Sessa WC, Pritchard KA Jr. Heat shock protein 90 and tyrosine kinase regulate eNOS NO* generation but not NO* bioactivity. *Am J Physiol Heart Circ Physiol*. 2004;286:H561–H569.
21. Konduri GG, Bakhutashvili I, Eis A, Pritchard K Jr. Oxidant stress from uncoupled nitric oxide synthase impairs vasodilation in fetal lambs with persistent pulmonary hypertension. *Am J Physiol Heart Circ Physiol*. 2007;292:H1812–H1820.
22. Konduri GG, Ou J, Shi Y, Pritchard KA Jr. Decreased association of HSP90 impairs endothelial nitric oxide synthase in fetal lambs with persistent pulmonary hypertension. *Am J Physiol Heart Circ Physiol*. 2003;285:H204–H211.
23. Zhou YQ, Foster FS, Nieman BJ, Davidson L, Chen XJ, Henkelman RM. Comprehensive transthoracic cardiac imaging in mice using ultrasound biomicroscopy with anatomical confirmation by magnetic resonance imaging. *Physiol Genomics*. 2004;18:232–244.
24. Pece-Barbara N, Vera S, Kathirkamathamby K, Liebner S, Di Guglielmo GM, Dejana E, Wrana JL, Letarte M. Endoglin null endothelial cells proliferate faster and are more responsive to transforming growth factor beta1 with higher affinity receptors and an activated Alk1 pathway. *J Biol Chem*. 2005;280:27800–27808.
25. Khoo JP, Zhao L, Alp NJ, Bendall JK, Nicoli T, Rockett K, Wilkins MR, Channon KM. Pivotal role for endothelial tetrahydrobiopterin in pulmonary hypertension. *Circulation*. 2005;111:2126–2133.
26. Nandi M, Miller A, Stidwill R, Jacques TS, Lam AA, Haworth S, Heales S, Vallance P. Pulmonary hypertension in a GTP-cyclohydrolase 1-deficient mouse. *Circulation*. 2005;111:2086–2090.
27. Tang JR, Markham NE, Lin YJ, McMurtry IF, Maxey A, Kinsella JP, Abman SH. Inhaled nitric oxide attenuates pulmonary hypertension and improves lung growth in infant rats after neonatal treatment with a VEGF receptor inhibitor. *Am J Physiol Lung Cell Mol Physiol*. 2004;287: L344–L351.
28. Wunderlich C, Schober K, Schmeisser A, Heerwagen C, Tausche AK, Steinbronn N, Brandt A, Kasper M, Schwencke C, Braun-Dullaeus RC, Strasser RH. The adverse cardiopulmonary phenotype of caveolin-1 deficient mice is mediated by a dysfunctional endothelium. *J Mol Cell Cardiol*. 2008;44:938–947.
29. Whitsett J, Martasek P, Zhao H, Schauer DW, Hatakeyama K, Kalyanaraman B, Vasquez-Vivar J. Endothelial cell superoxide anion radical generation is not dependent on endothelial nitric oxide synthase-serine 1179 phosphorylation and endothelial nitric oxide synthase dimer/monomer distribution. *Free Radic Biol Med*. 2006;40:2056–2068.
30. Zhao YY, Zhao YD, Mirza MK, Huang JH, Potula HH, Vogel SM, Brovkovych V, Yuan JX, Wharton J, Malik AB. Persistent eNOS activation secondary to caveolin-1 deficiency induces pulmonary hypertension in mice and humans through PKG nitration. *J Clin Invest*. 2009; 119:2009–2018.
31. Luo JD, Wang YY, Fu WL, Wu J, Chen AF. Gene therapy of endothelial nitric oxide synthase and manganese superoxide dismutase restores delayed wound healing in type 1 diabetic mice. *Circulation*. 2004;110:2484–2493.
32. Aschner JL, Foster SL, Kaplowitz M, Zhang Y, Zeng H, Fike CD. Heat shock protein 90 modulates endothelial nitric oxide synthase activity and vascular reactivity in the newborn piglet pulmonary circulation. *Am J Physiol Lung Cell Mol Physiol*. 2007;292:L1515–L1525.
33. Montani DP, LC, Girerd B, Chinet T, Lacombe P, Simonneau G, Humbert M. Fatal rupture of pulmonary arteriovenous malformation in hereditary hemorrhagic telangiectasia and severe PAH. *Eur Respir Rev*. 2009:42–46.
34. Shovlin CL, Tighe HC, Davies RJ, Gibbs JS, Jackson JE. Embolization of pulmonary AVMs: no consistent effect on pulmonary artery pressure. *Eur Respir J*. 2008.
35. Liu D, Wang J, Kinzel B, Mueller M, Mao X, Valdez R, Liu Y, Li E. Dosage-dependent requirement of BMP type II receptor for maintenance of vascular integrity. *Blood*. 2007;110:1502–1510.
36. Hong KH, Lee YJ, Lee E, Park SO, Han C, Beppu H, Li E, Raizada MK, Bloch KD, Oh SP. Genetic ablation of the BMPR2 gene in pulmonary endothelium is sufficient to predispose to pulmonary arterial hypertension. *Circulation*. 2008;118:722–730.
37. Mache CJ, Gamillscheg A, Popper HH, Haworth SG. Early-life pulmonary arterial hypertension with subsequent development of diffuse pulmonary arteriovenous malformations in hereditary haemorrhagic telangiectasia type 1. *Thorax*. 2008;63:85–86.

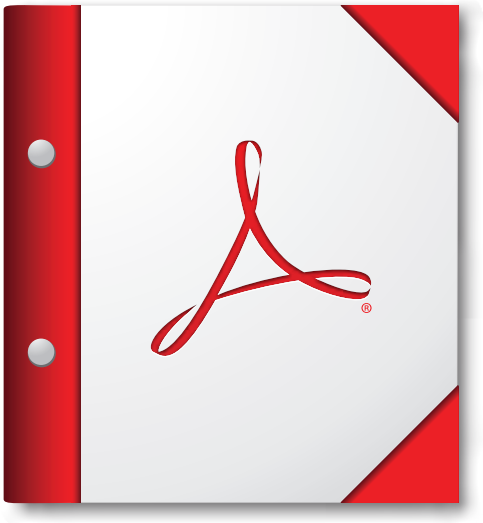

For the best experience, open this PDF portfolio in Acrobat 9 or Adobe Reader 9, or later.

Get Adobe Reader Now!